

Omentum ECM-based hydrogel as a platform for cardiac cell delivery

This content has been downloaded from IOPscience. Please scroll down to see the full text.

2015 Biomed. Mater. 10 034106

(<http://iopscience.iop.org/1748-605X/10/3/034106>)

View [the table of contents for this issue](#), or go to the [journal homepage](#) for more

Download details:

This content was downloaded by: tdvir

IP Address: 132.66.11.212

This content was downloaded on 14/05/2015 at 06:02

Please note that [terms and conditions apply](#).

Biomedical Materials



PAPER

Omentum ECM-based hydrogel as a platform for cardiac cell delivery

RECEIVED
11 December 2014

REVISED
18 March 2015

ACCEPTED FOR PUBLICATION
23 March 2015

PUBLISHED
13 May 2015

Michal Shevach^{1,2}, Rotem Zax¹, Alona Abrahamov¹, Sharon Fleischer^{1,2}, Assaf Shapira¹ and Tal Dvir^{1,2,3}

¹ The Laboratory for Tissue Engineering and Regenerative Medicine, Department of Molecular Microbiology and Biotechnology, George S. Wise Faculty of Life Science, Tel Aviv University, Tel Aviv 69978, Israel

² The Center for Nanoscience and Nanotechnology, Tel Aviv University, Tel Aviv 69978, Israel

³ Department of Materials Science and Engineering, Tel Aviv University, Tel Aviv 69978, Israel

E-mail: tdvir@post.tau.ac.il

Keywords: cell delivery system, decellularized, extracellular matrix, hydrogel, omentum, tissue engineering

Supplementary material for this article is available [online](#)

Abstract

Cardiovascular diseases remain the number one killer in Western countries. Despite recent advances and promising results in cardiac cell-based therapy, one of the remaining challenges is poor cell retention in the desired site. As a solution, cell delivery systems are developed to ensure that a sufficient number of viable cells reach the infarct area. These delivery systems are based on biomaterials that provide a surrogate microenvironment for the encapsulated cells, retaining them in the desired location post-delivery. Injectable thermoresponsive ECM-based hydrogels have been developed to achieve this goal. Unfortunately, the use of allogeneic or xenogeneic ECM may hamper the treatment due to an immune response to residual cellular content from the host. In this work, we have developed an omentum-based hydrogel capable of self-assembly under physiological conditions. Although in this study the omentum was obtained from porcine sources, it can be easily and safely extracted from the patient, serving as an autologous protective vehicle for the transported cells. We have characterized the biochemical composition, mechanical properties, and gelation and degradation kinetics of the processed biomaterial. Furthermore, the ability of the hydrogel to encapsulate cardiac cells and support their culture was evaluated. We envision that the newly developed platform may open new opportunities for personalized cell delivery to the heart and other tissues.

1. Introduction

Cardiovascular diseases remain the leading cause of morbidity and mortality in Western countries, as well as a significant healthcare economic burden [1]. More than one million myocardial infarctions (MIs) occur annually in the US alone, and more than five million patients are affected by congestive heart failure (CHF) [2]. An MI occurs when a blood vessel leading blood to the cardiac muscle is blocked, most commonly due to atherosclerotic plaque [3]. Cell necrosis rapidly occurs, followed by ischemic death of cardiac cells. Eventually, after ventricular remodeling within and near the affected area, a non-contracting collagenous scar tissue is formed. This results in decreased cardiac function, which may lead to CHF and death. Currently, the only clinically relevant solution for these end-stage patients is

heart transplantation. As heart donors are scarce, alternative therapies have attracted much attention in recent years.

One potential therapeutic strategy for cardiac muscle regeneration is the delivery of cells into the affected area [3]. Various cell types have been utilized for this purpose, including bone marrow derived stem cells [4], mesenchymal stem cells [5, 6], skeletal myoblasts [7] and cardiac stem cells [8]. However, the success of this therapy is jeopardized due to poor accumulation and retention of cells in the scar tissue [9, 10]. Furthermore, as the conditions in the infarcted area, such as poor oxidation and the presence of apoptotic and necrotic cells, jeopardize the viability of the delivered cells, the injected cells fail to form cell–cell or cell–matrix interactions and do not survive [10]. To address this problem, cells are pre-encapsulated into a delivery vehicle prior to injection

[3, 11]. The delivery vehicle provides a supporting microenvironment until the cells are integrated with the myocardium and degrades after a short period. A prerequisite of the encapsulating biomaterial is its biocompatibility, namely its compatibility with the encapsulated cells as well as with the host.

Hydrogels are ideal candidates to serve as cell delivery systems, as they can be fabricated from various compatible, cell-supporting biomaterials and their chemical and physical properties can be relatively easily tailored for the desired use [12]. Utilization of *in situ* polymerizing hydrogels can exploit the catheter delivery method for a relatively non-invasive procedure for the patient [13]. These unique hydrogel systems can be delivered to the desired site while remaining in the solution-like state, and then undergo a transition to a gel state under physiological conditions [14]. A variety of naturally and synthetically-derived materials, such as alginate [15], collagen [16], fibrin [17], and poly(N-isopropylacrylamide-co-acrylic acid) [18] have been studied as injectable cell carriers and have shown to regenerate the infarcted heart [19, 20].

The use of a soluble form of biologically-derived decellularized ECM (dECM) for *in situ* forming hydrogels has gained interest in recent years [21]. After tissue collection, the cellular material is removed by physical, chemical and enzymatic methods, and the dECM is solubilized into a liquid form. ECM-based hydrogels are composed of a variety of biological molecules, such as collagens, proteoglycans, glycosaminoglycans (GAGs) and growth factors (GFs), providing the encapsulated cells with a more biologically relevant microenvironment compared to hydrogels synthesized from the above materials. Decellularized allogeneic and xenogeneic pericardium [22, 23], urinary bladder [24], adipose [25], brain and spinal cord [26, 27], dermal [28] and other tissues have been studied as a source for ECM-based hydrogels. These hydrogels are thermosensitive, remaining soluble while at room temperature (RT), and gel in the body. Although the cellular content is removed prior to the ECM usage, the remaining matrix antigens may provoke an immunogenic response after transplantation [29–32].

Recently, we reported on the utilization of the omental matrix as a platform for engineering autologous functional cardiac patches [33, 34]. The omentum, a double sheet of highly vascularized peritoneum, can be easily, quickly and safely extracted from patients without health implications [35–37] and the processed biomaterial can be implanted without provoking an inflammatory response. In this study, we further processed the decellularized omental matrix to serve as thermoresponsive hydrogel for cell delivery. We have investigated the biochemical composition, mechanical properties, degradation kinetics and evaluated the biomaterial's potential to serve as a delivery vehicle of cardiac cells. Theoretically, with the patient's own cells and biomaterial, this therapeutic approach may become personalized.

2. Materials and methods

2.1. Decellularization of the omentum

The omentum was decellularized as previously reported [33]. Briefly, omenta of healthy six-month-old pigs were purchased from the institute of animal research in Kibutz Lahav, Israel. In order to remove the cells, the tissues were first agitated in hypotonic buffer and then subjected to gradual lipid extraction. Subsequently, the samples were again treated with the hypotonic buffer, followed by 0.5% (w/v) sodium dodecyl sulfate (SDS) washes. Next, the tissues were gently agitated with 40 units mL⁻¹ of Benzonase® nuclease (Novagen, Madison, WI). Finally, the tissues were rinsed with sterile phosphate-buffered saline (PBS), followed by sterile double distilled water, frozen overnight and lyophilized.

2.2. Preparation of solubilized omentum dECM

After lyophilization, the decellularized omentum was ground into a coarse powder using a Wiley Mini-Mill and then frozen until further use. Dry, milled omentum dECM was enzymatically digested by adding a 1 mg mL⁻¹ solution of pepsin (Sigma, 3200–4500 units mg⁻¹ protein) in 0.1 M HCl [22, 24]. The final concentration of dECM was varied between 1 and 1.5% (w/v). The dECM was digested for 64–72 h at RT under constant stirring until the liquid was homogenous with no visible particles. Subsequently, the salt concentration was adjusted using PBSx10 and the pH was raised to 7.2–7.4 using 1 M NaOH. Raising the pH terminates pepsin activity (the enzyme is deactivated above pH 6 [38]). To induce gelation *in vitro*, the solubilized omentum ECM was placed in a humidified cell incubator with 5% CO₂, at 37 °C.

2.3. Histology and biochemical analysis

Liquidated omentum dECM was allowed to gel for 2 h at 37 °C. Subsequently, gelled samples and native omental samples were fixed in optimum cutting temperature (O.C.T.) embedding medium (Tissue-Tek, Sakura, Japan), sections of 10–12 μm were obtained using a Cryotome™ FSE (Thermo Scientific), and affixed on X-tra® adhesive glass slides (Leica Biosystems, Wetzlar, Germany). Hematoxylin and Eosin (H and E) staining (Merck, Geneva, Switzerland) for decellularization confirmation and Masson's trichrome (Bio-Optica, Milano, Italy) for cell and collagen detection staining were performed according to the manufacturer's guidelines. For Sodium Dodecyl Sulfate Polyacrylamide Gel Electrophoresis (SDS-PAGE) protein analysis, 100 μl of 5% SDS solution were added to an equal volume of 1 or 1.5% omentum hydrogels. The mixture was incubated for 10 min at RT for sample solubilization, after which 7.5 μl of each sample (equal to 75 and 112.5 μg of the 1 and 1.5% liquidated dECM, respectively) were taken and separated alongside a PageRuler® size marker (Thermo Scientific, Waltham, MA) on Tris-glycine SDS-polyacrylamide gel

(12%). Protein bands were visualized using SeeBand Forte®Protein staining solution (Gene Bio application, Israel). For nucleic acid detection, slides were stained with $5 \mu\text{g mL}^{-1}$ Hoechst 33258 (Sigma-Aldrich) for 7 min, followed by washes with PBS. The samples were visualized using an inverted fluorescence microscope (Nikon Eclipse TI) and images were taken under the same exposure parameters. DNA was extracted from dried native or lyophilized dECM hydrogel samples according to the manufacturer's guidelines (DNeasy Blood and Tissue Kit, Qiagen, Hilden, Germany). The obtained DNA was quantified by measurements of the optical density (OD) at 260 nm wavelength using spectrophotometer (Nanodrop 1000, Thermo Scientific). The GAGs content per sample was determined in dried native or lyophilized hydrogels using the Blyscan sulfated GAG assay kit (Biocolor Ltd, UK) according to the manufacturer's instructions.

2.4. Scanning electron microscopy

For scanning electron microscope (SEM) imaging, samples of 1 and 1.5% liquidated dECM were allowed to gel for 2 h. The samples were then fixed with 2.5% glutaraldehyde in PBS for 2 h at RT followed by dehydration using a graded series of ethanol–water solutions (50–100%). Liquidated dECM samples were dried overnight using a vacuum desiccator at RT. Finally, all samples were critical point dried, sputter-coated with gold and observed under SEM (Jeol JSM840A). The properties of the fibers from at least 5 different randomly located images of each hydrogel were measured with ImageJ software (NIH).

2.5. Gelation kinetics

Gelation kinetics was evaluated using spectrophotometer turbidity, as previously described [39]. Briefly, $500 \mu\text{l}$ of 4°C liquidated dECM samples at different concentrations were transferred to 48-well plates. Absorbance was measured every minute for 3 h at 405 nm wavelength, using a Synergy™ Multi-Detection Microplate Reader (BioTek, Winooski, VT), preheated to 37°C [40]. Absorbance values were normalized and plotted over time. A linear fit was applied to the linear region of the normalized curves to calculate the maximum slope of gelation (S), the half-time of gelation ($T_{0.5}$) and the lag phase (T_{lag}). The half-time of gelation was defined as the time when the material reached 50% of the maximum measured absorbance. The lag phase was calculated by finding the time at which the linear fit was zero for normalized absorbance [39].

2.6. Rheological properties

Rheological experiments were performed using a Discovery HR-3 hybrid Rheometer (TA Instruments, DE) with 8 mm diameter parallel plate geometry with a Peltier plate to maintain the sample temperature. The samples were loaded into the rheometer with the Peltier plate maintaining a temperature of 4°C . The

sample was protected from evaporation by applying mineral oil. The temperature was then set to 37°C to induce gelation; during this time the oscillatory moduli of the sample were monitored continuously at a fixed frequency of 1 Hz and a strain of 5%.

The final viscoelastic properties of the gel were measured by performing a frequency sweep between 0.04 and 10 Hz at 0.63% strain on samples that were allowed to gel for 24 h at 37°C . Data were best-fit to the following equation

$$\eta = kf^n \quad (1)$$

where (η) is the complex viscosity, (f) is frequency and (k) and (n) being constants [39, 41].

2.7. Swelling ratio

The 1 and 1.5% w/v liquid dECM were allowed to gel for 2 h in a plastic mold at 37°C . Then, 8 mm samples were punctured from the mold and allowed to swell in 3 ml culture medium (as described in section 2.9) in a 6-well plate, one scaffold per well, in a humidified CO_2 cell incubator at 37°C . Samples were collected after swelling times of 30 min, 24 and 72 h and the swollen weight (W_s) was measured at each time point. Next, scaffolds were frozen, lyophilized and measured again to obtain dry weight (W_d). Finally, the swelling ratios of the scaffolds were determined using the equation (2) [39]:

$$\frac{W_s - W_d}{W_d} \quad (2)$$

2.8. Enzymatic degradation assay

The 1 and 1.5% w/v liquidated dECM were allowed to gel for 2 h in a plastic mold at 37°C . Then, 8 mm samples were punctured from the mold and placed in a 24-well plate, one scaffold per well. Then, $500 \mu\text{l}$ solution of 1 U mL^{-1} collagenase type II (Worthington Biochemical Corporation, Lakewood, NJ) in Dulbecco's modified Eagle Medium (DMEM) were added to each well and scaffolds were placed in a humidified CO_2 cell incubator at 37°C under mild shaking conditions. Untreated scaffolds placed under the same conditions but without collagenase supplementation served as control. Solutions were changed every other day. Samples were collected after degradation times of 30 min, 24, 72 and 120 h, frozen and lyophilized. The remaining weight ratios of the scaffolds were determined using equation (3) [42]:

$$100 - \frac{(W_{\text{control}} - W_{\text{collagenase}})}{W_{\text{control}}} \cdot 100. \quad (3)$$

2.9. Cardiomyocytes isolation, encapsulation and culture

The left ventricles of 0–3 d-old neonatal Sprague–Dawley rats were harvested and the cells were isolated using 6 cycles (30 min each) of enzyme digestion with collagenase type II (95 U mL^{-1}) and pancreatin (0.6 mg mL^{-1} ; Sigma-Aldrich) in DMEM as previously reported [43]. After each round of digestion, cells were centrifuged (600 g, 5 min) and

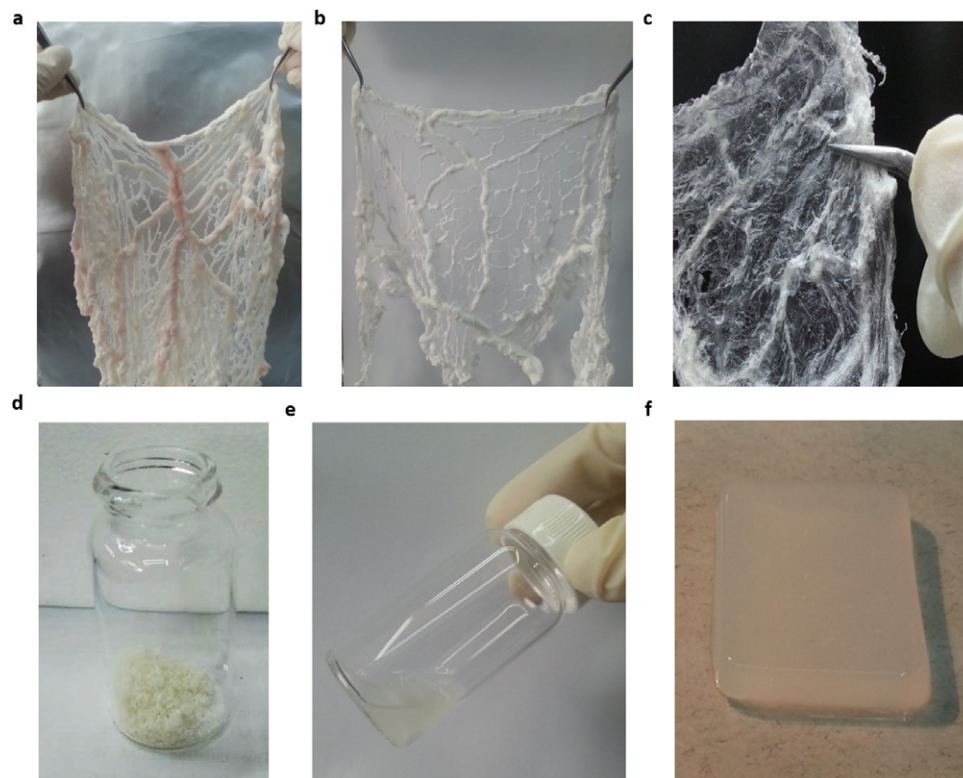


Figure 1. Decellularization and gelation process. (a) Fresh omentum prior to cell removal. Omentum during (b) and after (c) complete decellularization and lyophilization. (d) Milled dECM powder. (e) Digested dECM remains liquid at RT. (f) Under physiological conditions, the digested dECM self-assembles into a structured hydrogel.

re-suspended in culture medium composed of M-199 (Biological Industries, Beit-Haemek, Israel) supplemented with 0.6 mM $\text{CuSO}_4 \cdot 5\text{H}_2\text{O}$, 0.5 mM $\text{ZnSO}_4 \cdot 7\text{H}_2\text{O}$, 1.5 mM vitamin B12, 500 U mL^{-1} penicillin and 100 mg mL^{-1} streptomycin, and 0.5% (v/v) fetal bovine serum (FBS). To enrich the cardiomyocytes population, cells were suspended in culture medium with 5% FBS and pre-plated twice for 30 min. The cells were counted and encapsulated in 1:1 hydrogel:culture medium mix. The mixture was then poured into a plastic mold and left to gel for 2 h at 37 °C in a 5% CO_2 humidified cell incubator. Following gelation, scaffolds were extracted from the mold and used for further analysis. Cells cultured on the top surface of pre-formed hydrogels were seeded using a single droplet and allowed to attach to the hydrogels for 2 h before culture medium was added.

2.10. Cardiomyocytes immunostaining

Immunostaining was performed as previously described [44]. Cardiac cells seeded on or encapsulated within the hydrogel constructs were fixed and permeabilized in cold methanol for 10 min and blocked with Super Block (ScyTek Laboratories, West Logan, UT) for 8 min at RT. After 3 washes with PBS, the samples were incubated for 1 h with primary anti α -sarcomeric actinin antibody (1:750, Sigma-Aldrich). Next, the samples were rinsed and incubated for 1 h with Alexa Fluor 647 conjugated goat anti-mouse antibody (1:500; Jackson, West Grove, PA). For

nuclei detection, the cells were incubated for 7 min with Hoechst 33258 and washed three times. Samples were visualized using a laser scanning confocal microscope (Nikon Eclipse Ni).

2.11. Hydrogel area change due to cell degradation

Cardiac cells (1×10^6 and 2×10^6) were encapsulated in 200 μl of 1 and 1.5% hydrogels. Hydrogel degradation was macroscopically evaluated after 4 and 7 d in culture. Unseeded hydrogels at both concentrations served as controls for all the measured time points [28].

2.12. Statistical analysis

Statistical analysis data are presented as means \pm standard deviation (SD). Univariate differences between the 1 and 1.5% hydrogels were assessed with Student's *t*-test. All analyses were performed using GraphPad Prism version 6.00 for Windows (GraphPad Software). $p < 0.05$ was considered significant.

3. Results and discussion

3.1. Overview on omental decellularization and hydrogel production

In order to evaluate the potential of omentum ECM-based hydrogels to serve as cell delivery systems, we first focused on omentum decellularization. Fresh pig omentum was collected and decellularized as previously described [33] to produce dry dECM (figures 1 (a)–(c)). The dry dECM product was further milled and digested

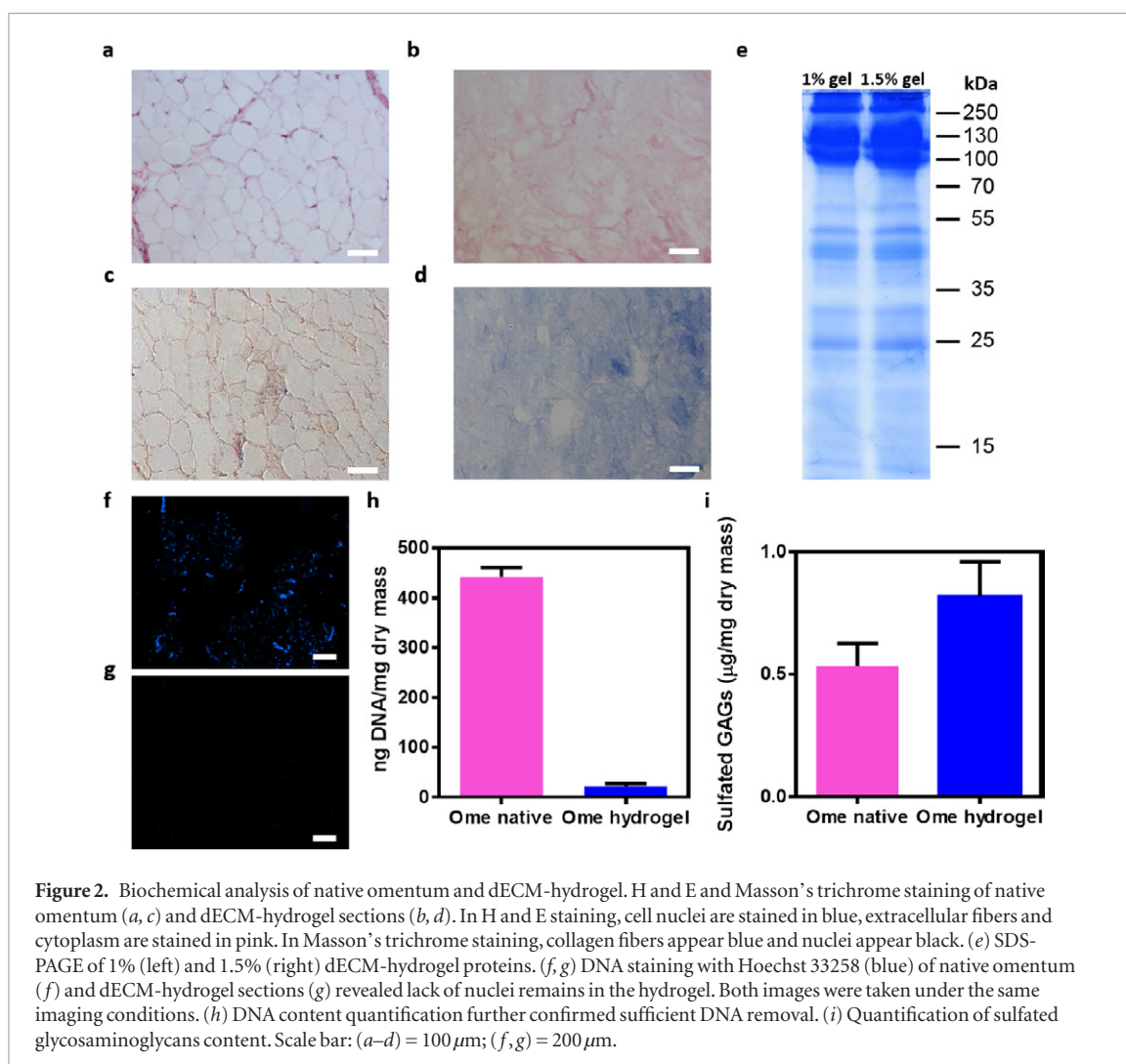


Figure 2. Biochemical analysis of native omentum and dECM-hydrogel. H and E and Masson's trichrome staining of native omentum (a, c) and dECM-hydrogel sections (b, d). In H and E staining, cell nuclei are stained in blue, extracellular fibers and cytoplasm are stained in pink. In Masson's trichrome staining, collagen fibers appear blue and nuclei appear black. (e) SDS-PAGE of 1% (left) and 1.5% (right) dECM-hydrogel proteins. (f, g) DNA staining with Hoechst 33258 (blue) of native omentum (f) and dECM-hydrogel sections (g) revealed lack of nuclei remains in the hydrogel. Both images were taken under the same imaging conditions. (h) DNA content quantification further confirmed sufficient DNA removal. (i) Quantification of sulfated glycosaminoglycans content. Scale bar: (a–d) = 100 µm; (f, g) = 200 µm.

to produce liquidated dECM (figures 1(d), (e)). Next, the solution was brought to physiological conditions using PBS × 10 and pH 7.2–7.4. The produced material could be easily injected at RT, but self-assembled into a structured mold maintaining hydrogel when allowed to gel at 37 °C (figure 1(f)).

3.2. Decellularization confirmation and biochemical analyses

We next sought to assess the removal of cellular content and the biochemical composition of the produced hydrogel. Histological H and E staining performed on native omentum (figure 2(a)) and dECM-hydrogel sections (figure 2(b)), showed complete cell removal as evident from the lack of cells and nuclei in the dECM-hydrogel sections. Masson's trichrome staining of native omentum (figure 2(c)) and dECM-hydrogel (figure 2(d)) revealed well-preserved, fibrous, collagen-rich content in the dECM-hydrogel sections. In the myocardium, cells are restrained by a complex network of structural proteins, such as collagen and elastic fibers, adhesive proteins like fibronectin and laminin and by a hydrated network of proteoglycans and GAGs [45]. The fibrillar collagen types I and III are the major

components of the myocardial collagen matrix. The interstitial collagen matrix surrounds and supports cardiac myocytes and the coronary microcirculation. High collagen content has an important role in ventricular mechanical function, cell attachment, alignment and coordinated force generation [46]. High collagen content found in the dECM-hydrogels can provide sufficient structural and biochemical support to the encapsulated cells, simulating the natural cardiac microenvironment during the course of scaffold degradation and cell integration with the healthy myocardium. SDS-PAGE has revealed protein bands between 250 to 15 kD, in both dECM solutions. Most protein bands were localized at similar positions as collagen I and other reported dECM-based digests, as was previously shown by Singelyn *et al* [22] and Freytes *et al* [24]. Complete DNA removal was further validated using Hoechst 33258 staining and residual DNA content quantification. Nuclei were detected in fresh omentum but not in the hydrogel sections (figures 2(f) and (g) respectively). DNA quantification revealed a significant reduction in DNA in the dECM-hydrogel (figure 2(h); less than 50 ng DNA per mg dry scaffold), which is considered as a completely decellularized material [47].

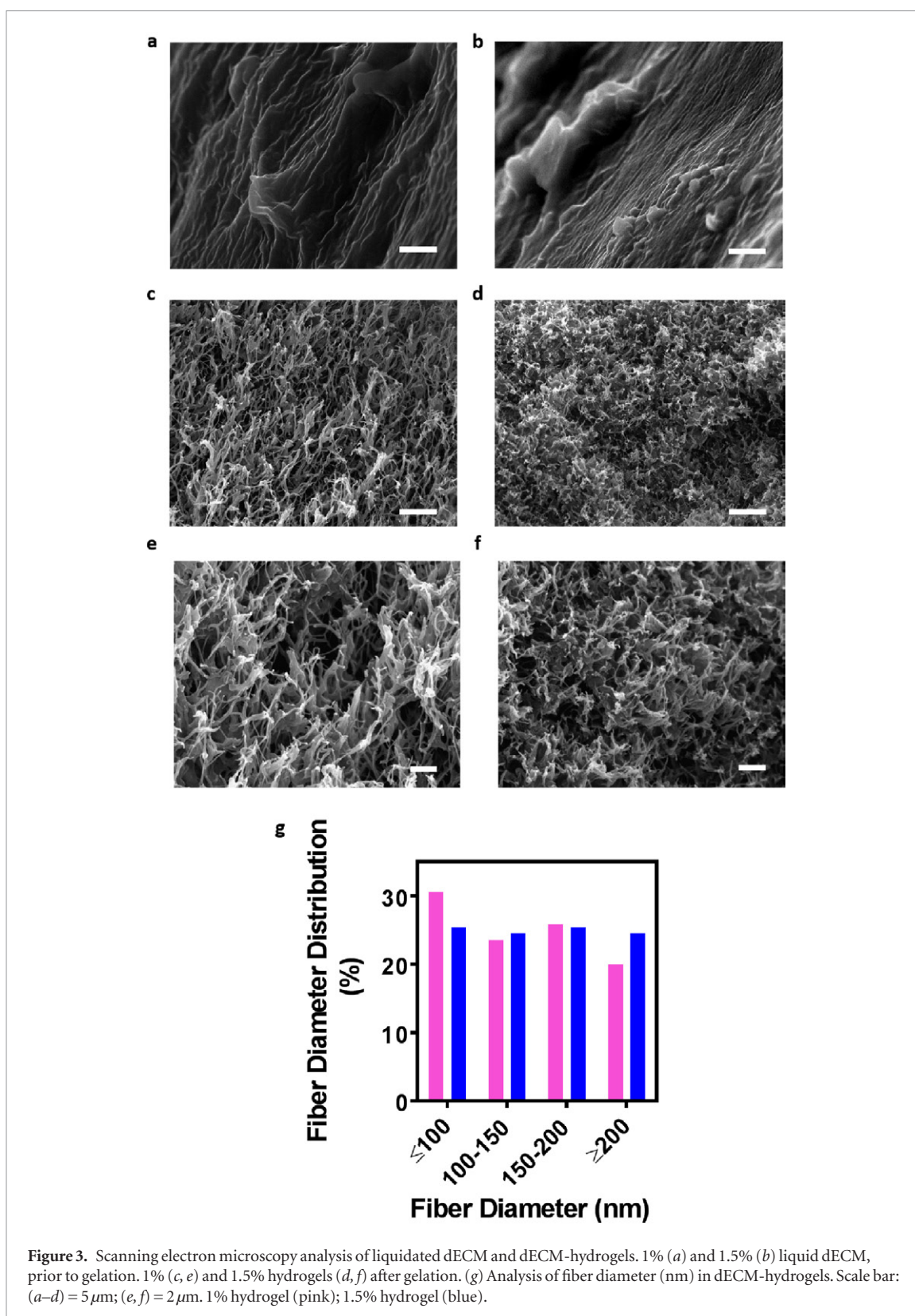


Figure 3. Scanning electron microscopy analysis of liquidated dECM and dECM-hydrogels. 1% (a) and 1.5% (b) liquid dECM, prior to gelation. 1% (c, e) and 1.5% hydrogels (d, f) after gelation. (g) Analysis of fiber diameter (nm) in dECM-hydrogels. Scale bar: (a–d) = 5 μm; (e, f) = 2 μm. 1% hydrogel (pink); 1.5% hydrogel (blue).

Complete removal of nuclei content is important to prevent immunogenicity of the autologous DNA released from omental resident cells during the decellularization process [48, 49].

GAGs are polysaccharides that are major components of the ECM. They control many biological processes, such as cell migration, proliferation and GFs protection [50, 51]. The preservation of GAG content

in the dECM-hydrogel could be beneficial for both encapsulated cell viability and for GFs encapsulation. Therefore, we sought to evaluate GAGs presence in the dECM-hydrogel. The remaining sulfated GAGs (sGAG) were quantified using Blyscan assay (figure 2(i)). The obtained results revealed that native omentum and dECM-hydrogels contained $0.53 \pm 0.09 \mu\text{g}$ and $0.82 \pm 0.14 \mu\text{g}$ sGAG per mg dry scaffold, respectively.

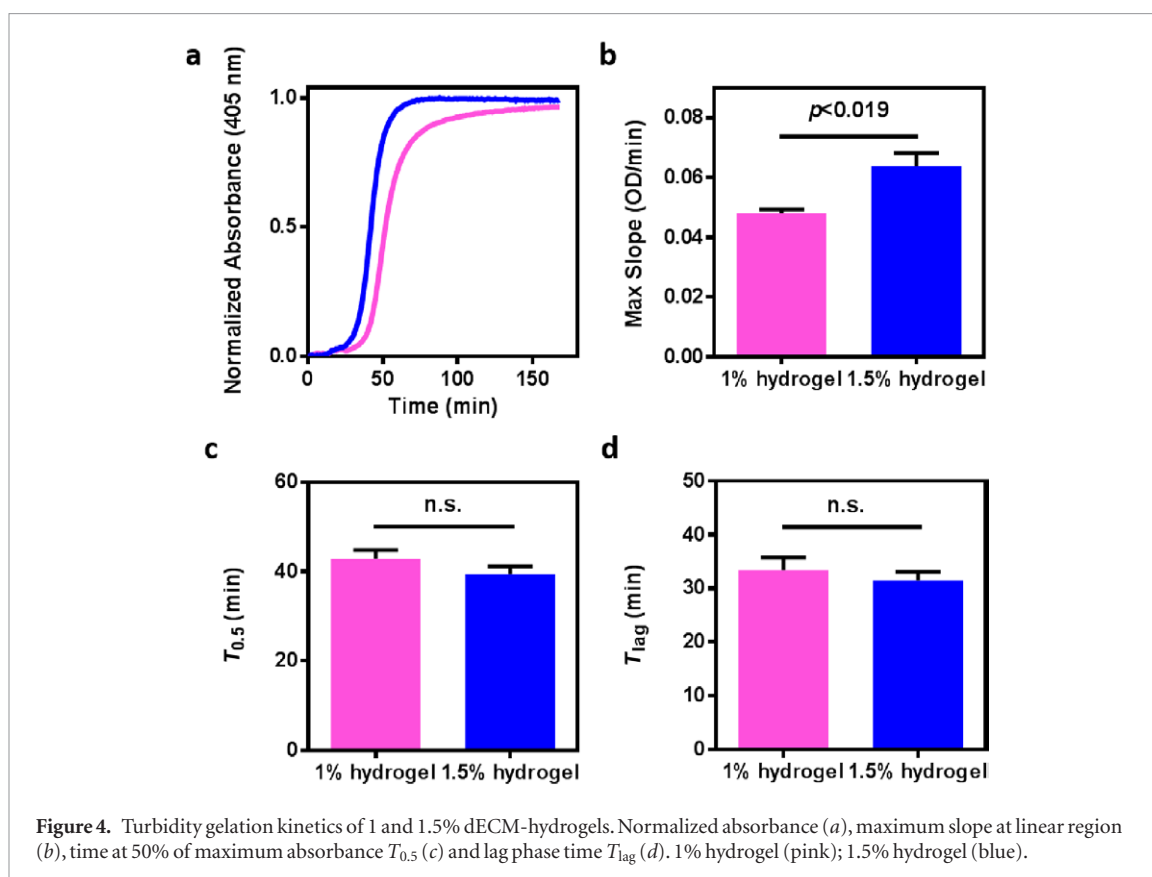


Table 1. Turbidity results for slope of linear region (S), half gelation time ($T_{0.5}$) and lag time (T_{lag}) of 1 and 1.5% dECM-hydrogels.

| Material | S (OD/min) | $T_{0.5}$ (min) | T_{lag} (min) |
|---------------|-------------------|------------------|------------------|
| 1% hydrogel | 0.048 ± 0.001 | 42.83 ± 1.93 | 33.45 ± 2.32 |
| 1.5% hydrogel | 0.064 ± 0.004 | 39.36 ± 1.88 | 31.54 ± 1.57 |

These findings are consistent with other reports of sGAG content in dECM-based digests [28, 34].

3.3. Scanning electron microscopy

To confirm fiber existence and analyze the fibrous structure, liquidated dECM and dECM-hydrogels were imaged using SEM. As shown, no fibers were visualized in liquidated dECM (figures 3(a) and (b)), whereas a complex network of fibers was revealed post gelation in both concentrations (figures 3(c)–(f)). As expected, the 1.5% dECM-hydrogel had a denser fibrillar structure compared to the 1% dECM-hydrogel. Both hydrogel concentrations showed randomly oriented fibers in the nanoscale region, usually between tens to hundreds nm in diameter (figure 3(g)). The average fiber diameter was around 150 nm in both the 1 and 1.5% concentrations. Such fiber dimensions are in accordance with endomysial fibers of the native cardiac matrix, which wrap individual cells and connect adjacent myocytes to one another [52, 53]. Therefore, this system could provide the structural signaling needed for encapsulated cell attachment and enhance their survival until the delivery vehicle is degraded and the cells are integrated within the desired location.

3.4. Turbidity gelation kinetics

Absorbance changes of liquidated dECM during the gelation period were used for calculating gelation kinetics parameters (figure 4). For both hydrogel concentrations a typical sigmoidal graph was observed after the temperature was elevated from 4 to 37 °C (figure 4(a)). Gelation parameters calculated from the obtained graphs (figures 4(b)–(d) and table 1) revealed that the higher concentration hydrogel (1.5% w/v) had a higher maximum slope in the linear region, reached half of maximum absorbance faster and had a shorter lag phase than the 1% w/v hydrogel. The gelation kinetics parameters, such as speed of gelation or lag time, can be controlled by varying the initial dECM concentration. These parameters influence the degree of cell, drug, GFs and hydrogel material leakage from the desired site to the adjacent areas after delivery, subsequently affecting the success of the treatment. Furthermore, as one of the advantages of the developed hydrogel is its injectability, gelation parameters might influence the final shape of the material inside the infarction and the time period the patient must remain static during the procedure.

3.5. Rheological properties of the dECM-hydrogels

Rheological properties of the obtained material are important characteristics in order to predict their behavior under applied forces. When the temperature was elevated from 4 to 37 °C and during the gelation period, both the storage modulus (G') and the loss modulus (G'') changed over time, and were characterized by a sigmoidal shape (figure 5(a) and supplementary

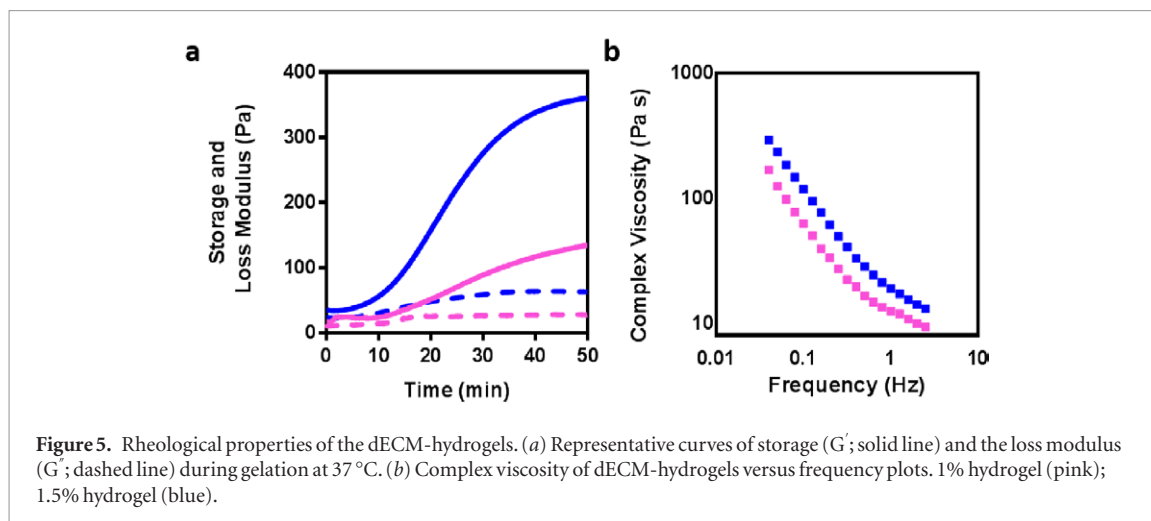


Figure 5. Rheological properties of the dECM-hydrogels. (a) Representative curves of storage (G' ; solid line) and the loss modulus (G'' ; dashed line) during gelation at 37 °C. (b) Complex viscosity of dECM-hydrogels versus frequency plots. 1% hydrogel (pink); 1.5% hydrogel (blue).

Table 2. Complex viscosity fit for dECM-hydrogels at different concentration.

| Material | k | n | R ² |
|---------------|---------------|----------------|----------------|
| 1% hydrogel | 12.799 ± 3.2 | - 0.694 ± 0.05 | 0.9574 |
| 1.5% hydrogel | 19.854 ± 2.05 | - 0.773 ± 0.01 | 0.9788 |

figure 1 (stacks.iop.org/BMM/10/034106/mmedia). As G' was greater than G'' at both concentrations throughout the measurements, the analyzed materials have pronounced elastic gel properties. Under the present conditions (5% strain, shear rate of 1 Hz), increasing material concentration from 1 to 1.5% w/v significantly increased the storage modulus, indicating the formation of stiffer gels. In addition, the kinetics of the storage and loss modulus was faster than the turbidity kinetics (figure 4 and table 1), consistent with previous results [24]. The complex viscosity of omentum dECM-hydrogels at both concentrations was assessed over a range of shear rates. Across all samples, the complex viscosity decreased as the shear rate increased (figure 5(b)). A linear trend was observed when obtained data was plotted on a log–log scale. As a result, the power equation was used to fit the data [39]. Increasing the concentration of the omentum-dECM increased intermolecular forces, resulting in an elevated viscosity. This increase in viscosity can be observed as a vertical shift of the data points in figure 5(b). This trend is confirmed by the increase of (k) values between the 1 and the 1.5% w/v samples (table 2). The (n) values across the samples are observed to be negative, which indicate that the material is shear thinning, meaning a material will have a lower viscosity under higher shear rates.

3.6. Swelling ratio by weight

Swelling studies indicated that a swelling equilibrium by mass was already reached at the first measured time point (30 min) for both hydrogel concentrations, remaining almost constant up to 7 d (figure 6(a)). At 30 min, a swelling equilibrium ratio of 43.59 ± 1.37 and 35.51 ± 0.08 was reached for the 1 and 1.5% dECM-hydrogel, respectively ($p = 0.02$). Swelling parameters

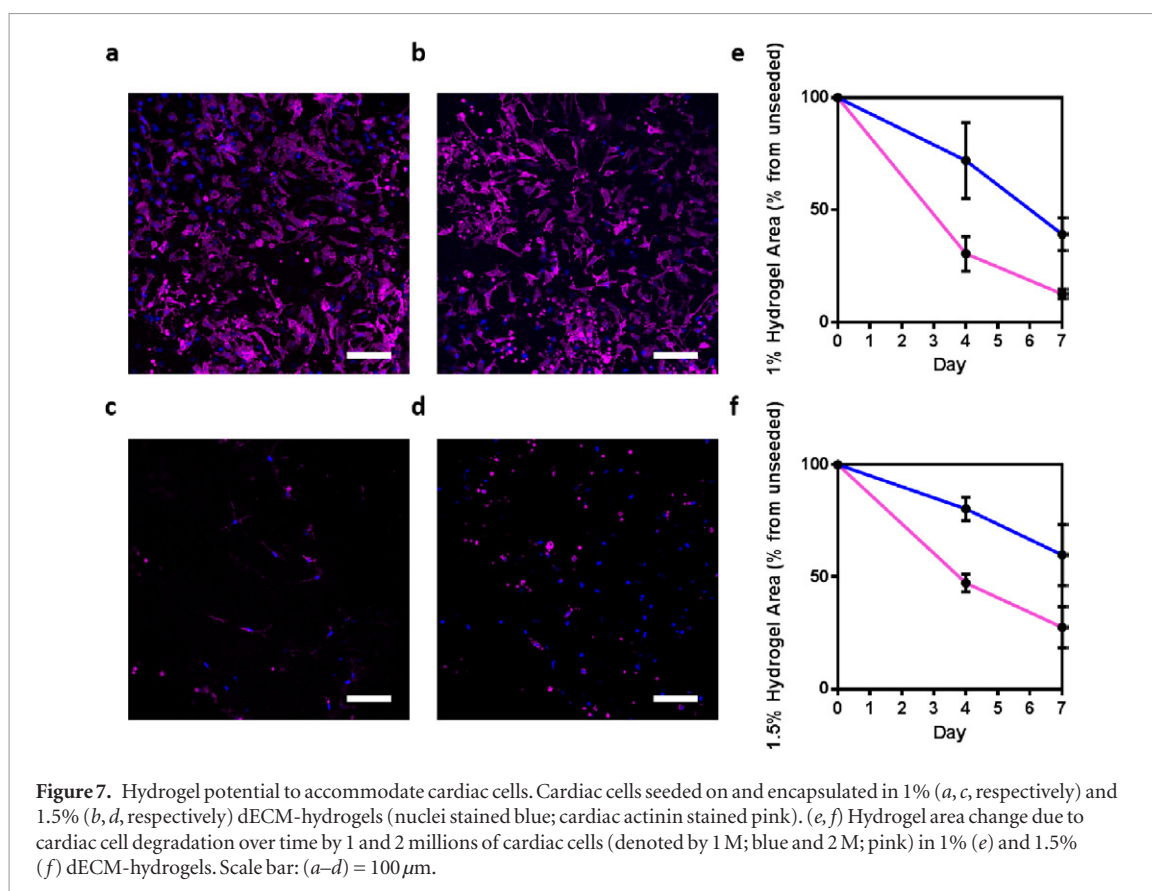
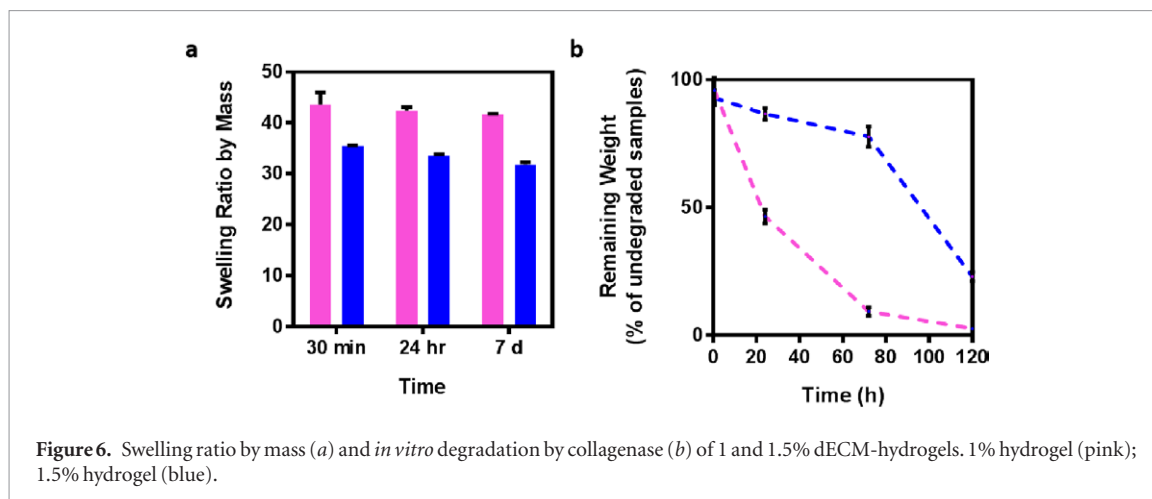
govern the degree of diffusion in and out of the hydrogel for various factors that influence both the encapsulated cells (oxygen and nutrients) and the surrounding environment (drugs or GFs). These parameters could influence the migration of encapsulated cells out of, or the degree of vascular cell infiltration into, the hydrogel. In addition, such swelling kinetics may be beneficial for hydrogel penetration into the scar tissue when it is in a liquid state, and later on after gelation and swelling, it may be detained and accumulated in the diseased area until its degradation.

3.7. Enzymatic degradation

As omentum dECM-hydrogels were developed for the purpose of cell delivery *in vivo*, we further examined the kinetics of hydrogel degradation by ECM-specific enzymes. In the myocardium, collagen fiber breakdown is mediated by collagenase, generally produced by cardiac fibroblasts [53, 54]. As expected, higher dECM concentration resulted in slower enzyme-dependent degradation (figure 6(b)). The degradation rate was similar through the first 30 min, however the 1.5% hydrogel degraded much more slowly throughout the rest of experiment. Comparatively, after 72 and 120 h, almost complete degradation was reached in the 1% hydrogel; while in the 1.5% hydrogels about 77 and 20% w/w still remained, respectively. These results indicate that degradation could be controlled through hydrogel concentration. The control over degradation kinetics is important as it influences encapsulated cell escape from the delivery vehicle, influences blood vessel infiltration into the matrix and GF or drug release from the formed hydrogels. All these parameters affect cell survival and consequently the therapeutic outcome from the treatment.

3.8. Hydrogel potential to accommodate cardiac cells

Finally, we sought to evaluate the ability of the hydrogel to support cardiac cells. Thus, cardiac cells were isolated and encapsulated within, or seeded on dECM-hydrogels (detailed in the *Materials and methods* section). On day 7 of cultivation, the cell–



hydrogel constructs were immunostained against cardiac actinin (figure 7). Cardiomyocytes seeded on top of the hydrogels appeared elongated with typical cardiac striations (figures 7(a) and (b)), similar to native myocardium [55]. We concluded that the successful adherence of cardiac cells to the matrix was due to binding domains still remaining in the hydrogel. Most cardiomyocytes encapsulated within the 1% hydrogel appeared elongated, although some cells did not spread and appeared round in shape (figure 7(c)). As for the encapsulated cells, more cells appeared rounded in the 1.5% (figure 7(d)) than in the 1% hydrogels. This could be explained by the relatively denser microenvironment inside the 1.5% hydrogel that could slow cell spreading.

Another important characteristic of cell–matrix interaction is the ability of the cells to degrade the encapsulating material. This is important in order to evaluate the cells' ability to be released from the matrix and consequently to be free to interact and integrate with the host tissue. After encapsulation, cells degrade the hydrogel, reducing hydrogel area over time [28]. We noticed that degradation was dependent both on initial encapsulated cell number and on hydrogel concentration (figures 7(e) and (f)). A higher cell number of initially encapsulated cells promoted a greater extent of degradation. We speculated that as the 1.5% hydrogels were found to be stiffer and denser than the 1% hydrogels, this hydrogel would degrade more slowly than the 1%. As expected, when the same number of cells was

encapsulated in both hydrogel concentrations, reduction in hydrogel area was slower for the 1.5% hydrogel. These results are consistent with previously reported data [28].

4. Summary and conclusions

One of the remaining challenges in cardiac regeneration therapy is sufficient cell retention after delivery [10]. Cell carriers that appropriately mimic the natural ECM cell microenvironment were developed in order to spatially retain viable cells in the delivery site. Injectable dECM-based hydrogels that self-assemble *in situ* under physiological conditions hold great promise as such delivery systems. Unfortunately, the biocompatibility of such hydrogels may be hampered by residual cellular content. Furthermore, encapsulation in autologous biomaterial might have a beneficial effect on the accommodation of cells from the same source. To overcome this limitation we have developed an omentum-based hydrogel that will not provoke an immune response after injection as this biomaterial can be easily and safely extracted from the patient and quickly processed to produce autologous dECM. We have shown that under physiological conditions, the liquidated dECM can form physical interactions and thus self-assemble into a shape-sustaining hydrogel. The developed dECM-hydrogel retained relevant aspects of the complex structure and biochemical composition of the ECM, such as fibrous architecture and high collagen and GAGs contents. We have validated that the mechanical properties, gelation and degradation kinetics of the developed hydrogel can allow the successful encapsulation and culture of cardiac cells. The developed platform, in combination with the patient's own cells could represent a new concept of patient-specific delivery systems for cardiac, as well as other, damaged tissues. Future work will focus on applying this method to other cell types, evaluating the developed platform for drug- and GF-sustained release and on evaluating the developed system for cardiac cell delivery in an MI animal model.

Acknowledgments

T D acknowledges support from the Moxie Foundation, European Union FP7 program (Marie Curie, CIG), Alon Fellowship, Israel Science Foundation and the Nicholas and Elizabeth Slezak Super Center for Cardiac Research and Biomedical Engineering at Tel Aviv University. M S thanks the NA' AMAT women's organization, Israel, for the NA' AMAT women's organization scholarship. This work is part of the doctoral thesis of M S. We would like to thank Dr Boaz Mizrahi and Ms Regina Kelmansky for their initial help with the rheology experiments.

References

- [1] Lloyd-Jones D *et al* 2010 Executive summary: heart disease and stroke statistics—update: a report from the American Heart Association *Circulation* **121** 948–54
- [2] Roger V L *et al* 2011 Heart disease and stroke statistics—update: a report from the American Heart Association *Circulation* **123** e18–209
- [3] Hastings C L, Roche E T, Ruiz-Hernandez E, Schenke-Layland K, Walsh C J and Duffy G P 2014 Drug and cell delivery for cardiac regeneration *Adv. Drug Deliv. Rev.* **84** 85–106
- [4] Orlic D *et al* 2001 Bone marrow cells regenerate infarcted myocardium *Nature* **410** 701–5
- [5] Amado L C 2005 *et al* Cardiac repair with intramyocardial injection of allogeneic mesenchymal stem cells after myocardial infarction *Proc. Natl Acad. Sci. USA* **102** 11474–9
- [6] Godier-Furnemont A F *et al* 2011 Composite scaffold provides a cell delivery platform for cardiovascular repair *Proc. Natl Acad. Sci. USA* **108** 7974–9
- [7] Farahmand P *et al* 2008 Skeletal myoblasts preserve remote matrix architecture and global function when implanted early or late after coronary ligation into infarcted or remote myocardium *Circulation* **118** S130–7
- [8] Ellison G M *et al* 2013 Adult c-kit(pos) cardiac stem cells are necessary and sufficient for functional cardiac regeneration and repair *Cell* **154** 827–42
- [9] Hudson W, Collins M C, deFreitas D, Sun Y S, Muller-Borer B and Kypson A P 2007 Beating and arrested intramyocardial injections are associated with significant mechanical loss: implications for cardiac cell transplantation *J. Surg. Res.* **142** 263–7
- [10] Malliaras K and Marban E 2011 Cardiac cell therapy: where we've been, where we are, and where we should be headed *Br. Med. Bull.* **98** 161–85
- [11] Wang C, Varshney R R and Wang D A 2010 Therapeutic cell delivery and fate control in hydrogels and hydrogel hybrids *Adv. Drug Deliv. Rev.* **62** 699–710
- [12] Borden B A, Yockman J and Kim S W 2010 Thermoresponsive hydrogel as a delivery scaffold for transfected rat mesenchymal stem cells *Mol. Pharm.* **7** 963–8
- [13] Sherman W, Martens T P, Viles-Gonzalez J F and Siminiak T 2006 Catheter-based delivery of cells to the heart *Nat. Clin. Pract. Cardiovasc. Med.* **3** S57–64 Suppl 1
- [14] Johnson T D and Christman K L 2013 Injectable hydrogel therapies and their delivery strategies for treating myocardial infarction *Expert Opin. Drug Deliv.* **10** 59–72
- [15] Leor J *et al* 2009 Intracoronary injection of *in situ* forming alginate hydrogel reverses left ventricular remodeling after myocardial infarction in Swine *J. Am. Coll. Cardiol.* **54** 1014–23
- [16] Dai W, Wold L E, Dow J S and Kloner R A 2005 Thickening of the infarcted wall by collagen injection improves left ventricular function in rats: a novel approach to preserve cardiac function after myocardial infarction *J. Am. Coll. Cardiol.* **46** 714–9
- [17] Christman K L, Fok H H, Sievers R E, Fang Q and Lee R J 2004 Fibrin glue alone and skeletal myoblasts in a fibrin scaffold preserve cardiac function after myocardial infarction *Tissue Eng.* **10** 403–9
- [18] Wall S T, Yeh C C, Tu R Y, Mann M J and Healy K E 2010 Biomimetic matrices for myocardial stabilization and stem cell transplantation *J. Biomed. Mater. Res. A* **95** 1055–66
- [19] Okada M, Payne T R, Oshima H, Momoi N, Tobita K and Huard J 2010 Differential efficacy of gels derived from small intestinal submucosa as an injectable biomaterial for myocardial infarct repair *Biomaterials* **31** 7678–83
- [20] Huang N F, Yu J, Sievers R, Li S and Lee R J 2005 Injectable biopolymers enhance angiogenesis after myocardial infarction *Tissue Eng.* **11** 1860–6
- [21] Singelyn J M and Christman K L 2010 Injectable materials for the treatment of myocardial infarction and heart failure: the promise of decellularized matrices *J. Cardiovasc. Transl. Res.* **3** 478–86
- [22] Singelyn J M, DeQuach J A, Seif-Naraghi S B, Littlefield R B, Schup-Magoffin P J and Christman K L 2009 Naturally derived myocardial matrix as an injectable scaffold for cardiac tissue engineering *Biomaterials* **30** 5409–16
- [23] Seif-Naraghi S B, Salvatore M A, Schup-Magoffin P J, Hu D P and Christman K L 2010 Design and characterization of an injectable pericardial matrix gel: a potentially autologous

- scaffold for cardiac tissue engineering *Tissue Eng. Part A* **16** 2017–27
- [24] Freytes D O, Martin J, Velankar S S, Lee A S and Badylak S F 2008 Preparation and rheological characterization of a gel form of the porcine urinary bladder matrix *Biomaterials* **29** 1630–7
- [25] Young D A, Ibrahim D O, Hu D and Christman K L 2011 Injectable hydrogel scaffold from decellularized human lipoaspirate *Acta Biomater.* **7** 1040–9
- [26] DeQuach J A, Yuan S H, Goldstein L S and Christman K L 2011 Decellularized porcine brain matrix for cell culture and tissue engineering scaffolds *Tissue Eng. A* **17** 2583–92
- [27] Medberry C J et al 2013 Hydrogels derived from central nervous system extracellular matrix *Biomaterials* **34** 1033–40
- [28] Wolf M T et al 2012 A hydrogel derived from decellularized dermal extracellular matrix *Biomaterials* **33** 7028–38
- [29] Badylak S F, Taylor D and Uygun K 2011 Whole-organ tissue engineering: decellularization and recellularization of 3D matrix scaffolds *Annu. Rev. Biomed. Eng.* **13** 27–53
- [30] Badylak S F, Freytes D O and Gilbert T W 2009 Extracellular matrix as a biological scaffold material: structure and function *Acta Biomater.* **5** 1–13
- [31] Badylak S F and Gilbert T W 2008 Immune response to biologic scaffold materials *Semin. Immunol.* **20** 109–16
- [32] Keane T J and Badylak S F 2014 The host response to allogeneic and xenogeneic biological scaffold materials *J. Tissue Eng. Regen. Med.* **9** 504–11
- [33] Shevach M, Soffer-Tsur N, Fleischer S, Shapira A and Dvir T 2014 Fabrication of omentum-based matrix for engineering vascularized cardiac tissues *Biofabrication* **6** 024101
- [34] Soffer-Tsur N, Shevach M, Shapira A, Peer D and Dvir T 2014 Optimizing the biofabrication process of omentum-based scaffolds for engineering autologous tissues *Biofabrication* **6** 035023
- [35] Thorne A, Lonnqvist F, Aelman J, Hellers G and Arner P 2002 A pilot study of long-term effects of a novel obesity treatment: omentectomy in connection with adjustable gastric banding *Int. J. Obes. Relat. Metab. Disord.* **26** 193–9
- [36] Merenda M, Litarski A, Kabzinski P and Janczak D 2013 Laparoscopic appendectomy as an alternative to conventional procedure—results in our own material *Polski przegląd chirurgiczny* **85** 323–8
- [37] Abe T, Kajiyama K, Harimoto N, Gion T and Nagaie T 2012 Laparoscopic omentectomy for preoperative diagnosis of torsion of the greater omentum *Int. J. Surg. Case Rep.* **3** 100–2
- [38] Johnston N, Dettmar P W, Bishwokarma B, Lively M O and Koufman J A 2007 Activity/stability of human pepsin: implications for reflux attributed laryngeal disease *Laryngoscope* **117** 1036–9
- [39] Johnson T D, Lin S Y and Christman K L 2011 Tailoring material properties of a nanofibrous extracellular matrix derived hydrogel *Nanotechnology* **22** 494015
- [40] Gelman R A, Williams B R and Piez K A 1979 Collagen fibril formation. Evidence for a multistep process *J. Biol. Chem.* **254** 180–6 (PMID: 758319)
- [41] Chan R W and Titze I R 1998 Viscosities of implantable biomaterials in vocal fold augmentation surgery *Laryngoscope* **108** 725–31
- [42] Holloway J L, Ma H, Rai R and Burdick J A 2014 Modulating hydrogel crosslink density and degradation to control bone morphogenetic protein delivery and *in vivo* bone formation *J. Control. Release* **191** 63–70
- [43] Shevach M, Maoz B M, Feiner R, Shapira A and Dvir T 2013 Nanoengineering gold particle composite fibers for cardiac tissue engineering *J. Mater. Chem. B* **1** 5210–7
- [44] Shevach M, Fleischer S, Shapira A and Dvir T 2014 Gold nanoparticle–decellularized matrix hybrids for cardiac tissue engineering *Nano Lett.* **14** 5792–6
- [45] Graham H K, Horn M and Trafford A W 2008 Extracellular matrix profiles in the progression to heart failure *European Young Physiologists Symp. Keynote Lecture (Bratislava, 2007)* *Acta Physiol. (Oxf.)* **194** 3–21
- [46] De Souza R R 2002 Aging of myocardial collagen *Biogerontology* **3** 325–35
- [47] Crapo P M, Gilbert T W and Badylak S F 2011 An overview of tissue and whole organ decellularization processes *Biomaterials* **32** 3233–43
- [48] Radic M 2014 Clearance of apoptotic bodies, NETs, and biofilm DNA: implications for autoimmunity *Front. Immunol.* **5** 365
- [49] Elliott M R and Ravichandran K S 2010 Clearance of apoptotic cells: implications in health and disease *J. Cell Biol.* **189** 1059–70
- [50] Raman R, Sasisekharan V and Sasisekharan R 2005 Structural insights into biological roles of protein-glycosaminoglycan interactions *Chem. Biol.* **12** 267–77
- [51] Linhardt R J and Toida T 2004 Role of glycosaminoglycans in cellular communication *Acc. Chem. Res.* **37** 431–8
- [52] Benedicto H G, Bombonato P P, Macchiarelli G, Stifano G and Prado I M 2011 Structural arrangement of the cardiac collagen fibers of healthy and diabetic dogs *Microsc. Res. Tech.* **74** 1018–23
- [53] Weber K T 1989 Cardiac interstitium in health and disease: the fibrillar collagen network *J. Am. Coll. Cardiol.* **13** 1637–52
- [54] Camelliti P, Borg T K and Kohl P 2005 Structural and functional characterisation of cardiac fibroblasts *Cardiovasc. Res.* **65** 40–51
- [55] Kohl P, Camelliti P, Burton F L and Smith G L 2005 Electrical coupling of fibroblasts and myocytes: relevance for cardiac propagation *J. Electrocardiol.* **38** 45–50